



Atmospheric deposition across the Atacama Desert, Chile: Compositions, source distributions, and interannual comparisons



Jianghanyang Li^a, Fan Wang^{b,c,*}, Greg Michalski^{a,d}, Benjamin Wilkins^d

^a Department of Earth, Atmospheric, and Planetary Sciences, Purdue University, West Lafayette, IN 47907, USA

^b School of Atmospheric Sciences, Guangdong Province Key Laboratory for Climate Change and Natural Disaster Studies, Sun Yat-sen University, Zhuhai 519082, China

^c Southern Marine Science and Engineering Guangdong Laboratory (Zhuhai), Zhuhai 519082, China

^d Department of Chemistry, Purdue University, West Lafayette, IN 47907, USA

ARTICLE INFO

Editor: Donald Porcelli

Keywords:

Atacama Desert
Atmospheric deposition
Interannual comparison
Sulfur isotopes

ABSTRACT

Hyper-arid areas such as the Atacama Desert accumulated significant amounts of insoluble dust and soluble salts from the atmosphere, providing minable salt deposits as well as mimicking the surface processes on Mars. The deposition rates, compositions and sources, however, were poorly constrained. Especially, the variabilities of atmospheric deposition in the Atacama Desert corresponding to a changing climate were unassessed. In this work, the atmospheric depositions collected using dust traps across a west-east elevation gradient in the Atacama (~23°S) from 1/2/2010 to 12/31/2011 were analyzed and compared to previous results in 2007–2009. The insoluble dust deposition rates in our sampling period were significantly higher than those of 2007–2009 in most dust traps, which was attributed to the changes in wind, highlighting the importance of long-term monitoring of insoluble dust fluxes. Soluble salts, instead, showed less distinct interannual variations in deposition rates, geochemical compositions or source contributions. At the coastal site (T1), soluble salts were originated from both primary sea-salt (SS) aerosols and non-sea-salt (NSS) sources such as anthropogenic emission, marine biogenic emission and biomass burning; the deposition rates of these salts largely depended on the wind speed and the amount of anthropogenic emissions. Sulfur isotopic evidence further showed that NSS sulfate at T1 was mainly originated from local SO₂ emission from local power plants. The inland sites (T2–T8) displayed much lower soluble salts deposition rates, and the salts were primarily sourced from entrainment of local surface minerals, including Na(Cl, NO₃), CaSO₄, and nitrate formed via atmospheric oxidation of anthropogenic NO_x. Sulfur isotopic compositions of sulfate deposited at T2–T8 were similar to those in local surface soil; however, three sites near the Chuquicamata mine showed slightly lower $\delta^{34}\text{S}_{\text{sulfate}}$ values, indicating the presence of secondary sulfate originated from mining activities. The soluble salts deposited at the Andean site (T10) were dominantly from wet deposition that incorporated local lake salts, and therefore, the deposition rates were mainly controlled by the amount of precipitation.

1. Introduction

As one of the driest places on Earth, the Atacama Desert has a hyperarid climate with mean annual precipitation (MAP) < 10 mm (Ericksen, 1981). The surface soil in the Atacama Desert is characterized by 1) very little organic matter content (Ericksen, 1981; Navarro-Gonzalez, 2003), 2) little to no microbial activity (Navarro-Gonzalez, 2003), 3) slow weathering, leaching, and water erosion rates (Ericksen, 1981; Ewing et al., 2006, 2008), and 4) a surface layer of desert pavement (Cooke and Warren, 1973; McFadden et al., 1987). In addition, high concentrations of soluble salts, such as nitrate, sulfate, chloride,

and perchlorate, have been found within Atacama soils (e.g., Rech et al., 2003; Bao et al., 2004). This is similar to the occurrences of nitrate salts (Kounaves et al., 2014; Stern et al., 2015), subsurface gypsum (CaSO₄·2H₂O) crusts (Edwards et al., 2005; Fishbaugh et al., 2007), massive chloride deposits (Osterloo et al., 2008), and abundant perchlorate (Hecht et al., 2009) on Mars (e.g., Catling et al., 2010; Navarro-Gonzalez, 2003; Vitek et al., 2012). Given the similar climatic conditions and soil chemical composition between the Atacama and Mars, the processes that led to the formation of these two unique planetary surfaces are possibly similar. Therefore, the Atacama Desert is considered as an ideal analog for studying the pedogenesis on Mars

* Corresponding author at: School of Atmospheric Sciences, Guangdong Province Key Laboratory for Climate Change and Natural Disaster Studies, Sun Yat-sen University, Zhuhai 519082, China.

E-mail address: wangfan25@mail.sysu.edu.cn (F. Wang).

<https://doi.org/10.1016/j.chemgeo.2019.07.037>

Received 16 February 2019; Received in revised form 16 July 2019; Accepted 30 July 2019

Available online 05 August 2019

0009-2541/ © 2019 Elsevier B.V. All rights reserved.

(e.g., Catling et al., 2010; Navarro-Gonzalez, 2003; Vitek et al., 2012).

The origins of the Atacama soil salts have long been debated (e.g., Darwin, 1906; Erickson, 1983 and references therein). While several studies have suggested that groundwater (~43–88 m below surface) played a significant role in the formation of some salt deposits in the Atacama Desert (Cameron and Leybourne, 2005; Pérez-Fodich et al., 2014; Álvarez et al., 2016), stable isotopic evidences have suggested that the majority of nitrate, sulfate and perchlorate ions in the Atacama top soil were produced photochemically in the atmosphere and then dry deposited as gases or dust (Bao et al., 2004; Böhlke et al., 1997; Michalski et al., 2004; Rech et al., 2003). Additionally, Wang et al. (2015) proposed a mechanism of soil accumulation via atmospheric deposition based on the meteoric ^{10}Be record of a 225 cm soil profile from the hyperarid core of the Atacama Desert, further suggesting atmospheric deposition is an important, even the dominant, process controlling soil development in the Atacama. Therefore, characterizing the rates, chemical compositions and sources of atmospheric deposition across the Atacama will help understand the soil development processes in the Atacama, with potential implications for a surface evolution mechanism on Mars.

Due to the lack of standard deposition monitoring stations, only a few studies have attempted to collect and analyze the atmospheric depositions in the Atacama. Ewing et al. (2006) first quantified the deposition rates of major ions (Na^+ , Ca^{2+} , NO_3^- , Cl^- and SO_4^{2-}) at three sites along a 300 km north-south transect and observed significant spatial variations in ion depositions. However, since these sites were all located the hyperarid core of the Atacama, whether they can represent the atmospheric deposition over the entire Atacama region was unclear. To fill this knowledge gap, Wang et al. (2014) set up a series of dust traps along a west-east transect from the Pacific coast to the Andean plateau and reported the chemical, mineral, and nitrate isotopic compositions of atmospheric deposition collected during 7/10/2007–12/31/2009 to characterize the atmospheric deposition along this transect.

However, a few questions still remain after this one-time recovery of atmospheric deposition over a 2.5-year sampling period. First, it is unclear whether the atmospheric depositions in the Atacama show interannual variations, which were observed in some other arid areas such as Southern California, U.S., Nevada, U.S., and Gansu, China (e.g., Reheis, 1997; Reheis and Kihl, 1995; Ta et al., 2004). Second, it is unknown how shifted climate conditions would affect the deposition in the Atacama. Last, there is little knowledge on the impact of anthropogenic activities (mainly mining and transportation) to the atmospheric deposition in the Atacama Desert. Thus, a follow-up comparison study to Wang et al. (2014) was necessary to examine and interpret the interannual variabilities of atmospheric deposition in the Atacama.

In this study, atmospheric depositions were collected during 1/2/2010–12/31/2011 by the same nine dust traps set up by Wang et al. (2014). The deposition rates as well as the chemical and isotopic compositions were analyzed and compared with the 2007–2009 results to investigate their interannual variations. These interannual comparisons can help understand the impact of climate, weather conditions and anthropogenic activities on the atmospheric deposition in the Atacama and assess the credibility of using annual average deposition to estimate the deposition over a longer period.

2. Sampling and analytical methods

The Atacama Desert, bordered on the west and by the Pacific Ocean on the east by the Andes, is divided into three physiographic provinces (Fig. 1A, from west to east): Coastal Range consisting of Mesozoic igneous and sedimentary rocks (Clarke, 2005), which runs in a general north-south direction adjacent to the Pacific Ocean with altitude < 2000 m; the Central Valley that is filled with Oligocene to Pliocene clastic sedimentary rocks (Sernageomin, 1982; Sillitoe et al., 1968) with altitude between 900 and 2500 m; and the Andes consisting of an altiplano about 4000 m in altitude and several intertwined pre-Andean

ranges and basins (e.g. the Atacama Basin, Clarke, 2005) that about the Andean Cordillera.

A series of nine dust traps were previously set up as shown in Fig. 1 (Wang et al., 2014) along a west-east transect in the Atacama: T1 on the Coastal Range, T2–T6 in the Central Valley, T7 on the pre-Andean range, T8 in the Atacama Basin and T10 on the Andes. Locations of dust traps were carefully selected to minimize the influence of anthropogenic activities, particularly open-pit mining activities that were widespread in the region. Each dust trap was made of a single-piece Bundt pan with the outer ring diameter of 25 cm and surface area of 477 cm². One piece of 0.25-inch-galvanized mesh was fixed on top of each pan, and a layer of glass marbles were spread on the mesh to simulate the effect of surface gravels in preventing wind erosion (Reheis and Kihl, 1995). The dust traps were all mounted ~1 m above ground to avoid the contamination from surface dust. Sample collection spanned from 1/2/2010 to 12/31/2011.

The sample collection and processing procedures were identical to those used for the 2007–2009 depositions in Wang et al. (2014). At the end of the exposure period, atmospheric deposition in each trap was carefully washed multiple times with Millipore water (18.2 MΩ·cm) into a 1 L plastic bottle, to ensure complete transferring of both insoluble and soluble material into the bottle. The solutions were then kept frozen, shipped to Purdue University, and freeze-dried to evaporate all the water. The residual solid materials were weighed, dissolved in ~100 mL Millipore water to make sure the major inorganic salts, i.e. (Na, K)(Cl, NO₃), (Na, K)₂SO₄, (Mg, Ca)SO₄²⁻, (Mg, Ca)(Cl, NO₃)₂, were far from being saturated. The re-washing solution was then filtered to separate soluble salts from insoluble dust. The insoluble dust was subsequently freeze-dried to ensure minimum volatilization and weighed to calculate the mass of soluble salts. Since the major inorganic salts were found undersaturated in the ~100 mL re-washing solutions, we suggest all the major ions have been completely dissolved, while some trace elements (e.g. Mn, Fe, Cu, Zn) forming low-solubility salts might not have been completely dissolved (Pan and Wang, 2015). However, the atmospheric fluxes of trace elements were generally 3–4 orders of magnitude lower than those of the major ions (Pan and Wang, 2015). Therefore, the contributions of trace elements to the total material deposition were minor, and their incomplete dissolution would not introduce significant uncertainties to the calculation of the insoluble/soluble material deposition rates here.

For cation (Na^+ , K^+ , Ca^{2+} , Mg^{2+}) analysis, 5 mL of each solution was mixed with 5 mL 10% HNO₃, then analyzed by ICP-OES (Thermo Scientific, Pittsburgh, PA, USA) in the Purdue Rare Isotope Measurement (PRIME) Laboratory at Purdue University. Another aliquot of each solution was used for anion (Cl^- , NO_3^- , SO_4^{2-}) analysis using a Dionex DX-500 Ion Chromatography (Dionex Corp., Sunnyvale, CA, USA) in the Purdue Stable Isotope Laboratory at Purdue University. For all ions at the T1 site, we calculated the enrichment factors (EF) relative to seawater by assuming all the Na^+ deposition in T1 was originated from seawater (Table 2, see Discussion):

$$\text{EF}_X = (\text{X}/\text{Na}^+)_{\text{T1}} / (\text{X}/\text{Na}^+)_{\text{seawater}}$$

in which $(\text{X}/\text{Na}^+)_{\text{T1}}$ represented the molar ratio of any ion (X) to Na^+ at T1 and $(\text{X}/\text{Na}^+)_{\text{seawater}}$ was the molar ratio of ion X to Na^+ in seawater (Pilson, 2012). EF values < 1 suggested biologic, chemical, or physical losses of ion X, and the loss of X was defined as X deficit: $\text{X deficit} = [\text{Na}^+]_{\text{T1}} \times (\text{X}/\text{Na}^+)_{\text{seawater}} - [\text{X}]_{\text{T1}}$. EF values > 1 indicated extra source(s) other than seawater for ion X, and the ion X was divided into sea-salt ion (SS-X) and non-sea-salt ion (NSS-X): $\text{SS-X} = [\text{Na}^+]_{\text{T1}} \times (\text{X}/\text{Na}^+)_{\text{seawater}}$; $\text{NSS-X} = [\text{X}]_{\text{T1}} - [\text{Na}^+]_{\text{T1}} \times (\text{X}/\text{Na}^+)_{\text{seawater}}$.

Sulfur isotopic analysis of soluble sulfate was performed at the Purdue Stable Isotope Laboratory. A 0.5 mL of 5% acidified BaCl₂ was added into 5 mL of each solution to completely precipitate sulfate as BaSO₄ that was then extracted, weighed, mixed with V₂O₅ powder, and combusted at 980 °C in a Costech Elemental Analyzer. The produced SO₂ was then directed to an isotope ratio mass spectrometer (IRMS-Thermo Delta V Plus) equipped with a ConFlo interface for isotopic

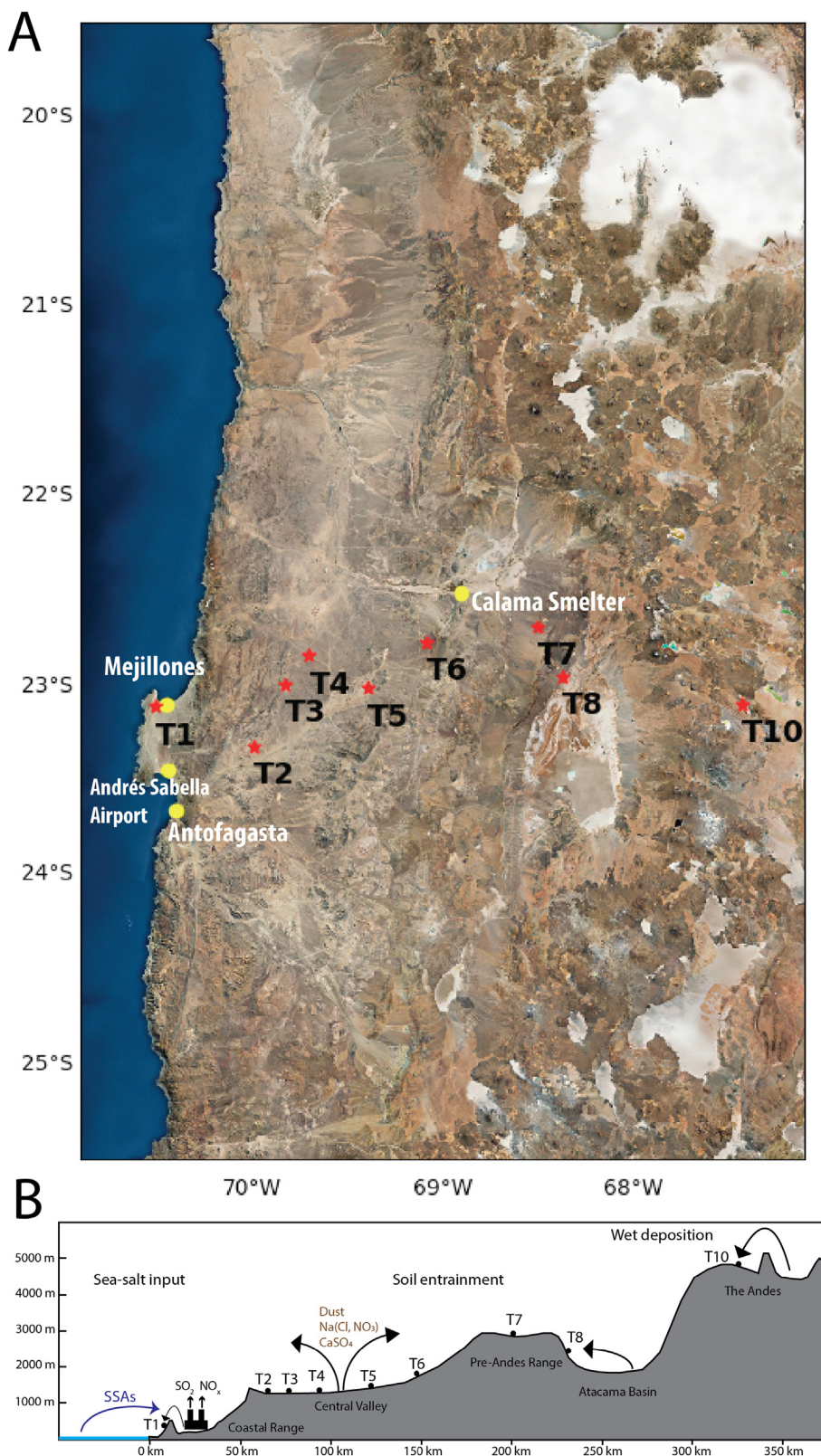


Fig. 1. Geological map (A) of the Atacama Desert showing the locations of dust traps, and the sketch of the transect (B) modified from Wang et al. (2014).

analysis. The sulfur isotopic compositions were reported in delta notation: $\delta^{34}\text{S} = ((^{34}\text{S}/^{32}\text{S})_{\text{sample}} / (^{34}\text{S}/^{32}\text{S})_{\text{reference}} - 1) * 1000\text{‰}$, in which the reference material is Vienna-Canyon Diablo Troilite (VCDT), the standard deviation (1σ) of our sulfur isotopic analysis was $\pm 0.2\text{‰}$.

3. Results

Bulk mass (insoluble dust and soluble salts) atmospheric deposition rates varied significantly along the west-east transect, with the lowest deposition rate of $4.3 \text{ g/m}^2/\text{yr}$ at T8 and the highest of $149.2 \text{ g/m}^2/\text{yr}$ at

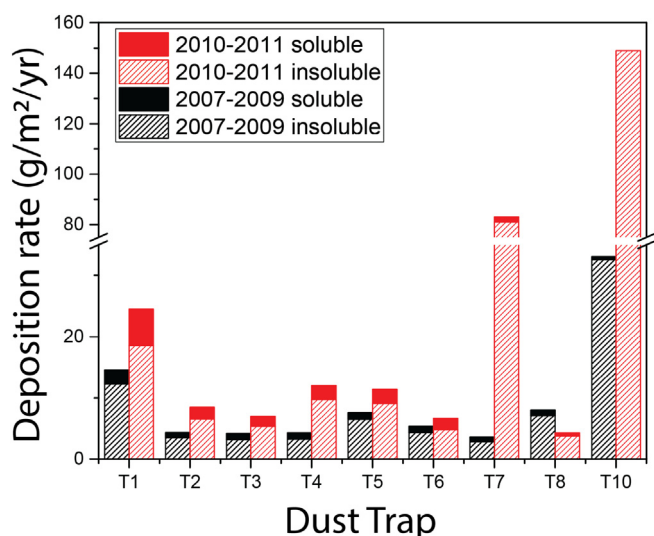


Fig. 2. Insoluble dust and soluble salts depositions of T1–T10 during both sampling periods.

T10 (Fig. 2). The spatial variations in the bulk mass deposition rates were mainly controlled by the insoluble dust deposition rates that spanned from 3.8 g/m²/yr to 149.0 g/m²/yr (Fig. 2). Dust traps in mountainous regions showed higher insoluble dust deposition rates: 18.5 g/m²/yr at T1, 80.9 g/m²/yr at T7 and 149.0 g/m²/yr at T10, while T2–T6 (Central Valley) and T8 (Atacama Basin) displayed lower insoluble dust deposition rates ranging from 3.8 g/m²/yr to 9.8 g/m²/yr. Comparing to the 2007–2009 period, the insoluble dust deposition rates in 2010–2011 increased by 11% to 2723%. The exception was T8, the insoluble dust deposition of which decreased by 47% from 7.1 g/m²/yr to 3.8 g/m²/yr (Fig. 2).

The deposition rates of soluble salts ranged from 0.2 to 6.0 g/m²/yr and displayed a general decreasing trend from T1 to T10 (Figs. 2 and 3). The coastal site (T1) had the highest soluble salts deposition rate (6.0 g/m²/yr) and the central depression (T2–T7) showed lower but consistent deposition rates ranging from 1.7 to 2.3 g/m²/yr. The lowest soluble salts deposition rates were at T8 and T10 (< 0.5 g/m²/yr). The soluble salts deposition rates also showed interannual variabilities. The 2010–2011 soluble salts deposition rates at T1 to T7 increased by 67%–176% relative to 2007–2009, while the rates in T8 and T10 decreased by 46% and 57%, respectively.

Major cations (Na⁺, Ca²⁺, K⁺, Mg²⁺) and anions (Cl⁻, NO₃⁻, SO₄²⁻) accounted for 47 ± 11% of total soluble salts in the dust traps (Table 1 and Fig. 3). Their deposition rates showed a similar spatial variation pattern as the soluble salts deposition rates. Among all the sites, T1 displayed the highest ion deposition rates, with the depositions of Na⁺, K⁺, NO₃⁻, Cl⁻ and SO₄²⁻ were 3 to 20 times higher than the other sites. T2–T7 sites had consistently lower ion deposition rates than T1, and the deposition rates of all ions were lowest at T8 and T10.

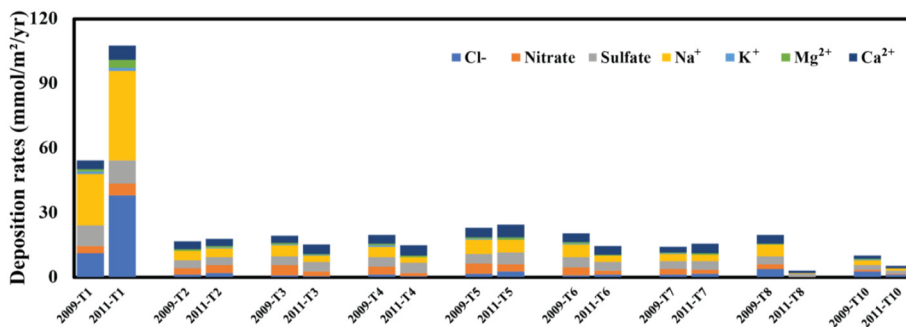


Fig. 3. Soluble ion deposition rates at T1–T10 sites during both sampling periods.

Compared to 2007–2009, the 2010–2011 total ion deposition (sum of Na⁺, Ca²⁺, K⁺, Mg²⁺, Cl⁻, NO₃⁻, SO₄²⁻, Fig. 3) was 98% higher at T1, 20%–85% lower at T3, T4, T6 and T8, and not significantly different at T2, T5 and T7.

The sulfur isotopic composition of soluble sulfate ($\delta^{34}\text{S}_{\text{sulfate}}$) in the nine dust traps ranged from 4.0‰ to 8.3‰ (Table 1, Fig. 5). The lowest $\delta^{34}\text{S}_{\text{sulfate}}$ value (4.0‰) occurred at T1 while T8 had the highest $\delta^{34}\text{S}_{\text{sulfate}}$ value of 8.3‰. The $\delta^{34}\text{S}_{\text{sulfate}}$ at T2–T4 were similar (7.1‰ to 7.6‰), and then showed a decreasing trend from 7.5‰ to 4.7‰ from T4 to T7. The Andean dust trap (T10) had the $\delta^{34}\text{S}_{\text{sulfate}}$ of 5.8‰.

4. Discussion

4.1. Coastal site T1

The deposition rate of insoluble dust at T1 had significant inter-annual variations, which could be attributed to variations in wind speed, precipitation, and/or anthropogenic activities. T1 was located on the west side of a hill slope, ~6 km away from the ocean. During 2010–2011, the deposition rate of insoluble dust (18.5 g/m²/yr) was 50% higher relative to that of 2007–2009 (12.3 g/m²/yr, Figs. 2 and 3). The insoluble dust at T1 had been hypothesized to be primarily from 1) entrainment of down slope dust, which was mainly weathered silicates, and 2) nearby surface and subsurface soil due to nearby open-pit mining activities (Wang et al., 2014). However, no significant geomorphology alteration was observed near the city of Mejillones during 2007–2011 (Sargent et al., 2010), therefore, dust from nearby open-pit mining activities should be minimal. Fluctuations in weather conditions, such as increased wind speed, would greatly increase the insoluble dust deposition by increasing the entrainment of particles from the surface (Goudie and Middleton, 1992; Reheis and Kihl, 1995; Shao et al., 1993). The wave height data off the coast supported a higher wind speed during 2010–2011 than 2007–2009. A buoy ~1500 km off the coast of Chile in Southern Pacific Ocean (Station 32ST0, National Data Buoy Center, 2018) measured hourly wave heights during both sampling periods. The average wave heights during 2010–2011 (2.42 ± 0.65 m) were higher than those of 2007–2009 (2.21 ± 0.60 m), corresponding to a ~0.5 m/s increase in average wind speed using the statistical wave forecasting equation (Group, 1988). Besides, the changes in wind speed was likely tied to the occurrence of El Niño since El Niño was suggested to reduce the average wind speeds and precipitation in northern and central Chile (Watts et al., 2017). 2007, 2008, 2010 and 2011 were all moderate to strong La Niña years, but 2009 was a moderate El Niño year (National Weather Service, 2015). Therefore, the average wind speed during 2010–2011 could be higher than during 2007–2009, possibly resulting in a higher dust deposition rate.

The soluble salts deposition rates at T1 had increased by 159% in 2010–2011 (6.0 g/m²/yr, Fig. 2) relative to 2007–2009 (2.6 g/m²/yr), and all the inorganic ion deposition rates increased, but to different extents (Table 1). The contributions of local soil to the soluble salt

Table 1

Deposition rates of soluble cations and anions (in mmol/m²/yr) and insoluble dust (in g/m²/yr) during 2010–2011, and their changes (in %) comparing to during 2007–2009, as well as the sulfur isotopic compositions.

Trap	Cl ⁻	NO ₃ ⁻	SO ₄ ²⁻	Na ⁺	K ⁺	Mg ²⁺	Ca ²⁺	Dust	Na ⁺ /(Cl ⁻ + NO ₃ ⁻)	Ca ²⁺ /SO ₄ ²⁻	Negative/positive	δ ³⁴ S (‰)
T1	38.0	5.6	10.4	41.9	1.2	3.8	6.7	18.5	0.96	0.64	1.01	4.0
Change (%)	244.1	62.3	9.2	75.1	23.9	208.4	62.2	50.8				
T2	2.1	3.6	3.6	4.2	0.2	0.9	3.2	6.5	0.75	0.88	1.02	7.6
	49.3	24.4	-1.7	2.7	10.9	9.4	-9.7	85.6				
T3	0.6	1.9	4.5	3.0	0.3	0.6	4.4	5.3	1.2	0.97	0.88	7.1
	-36.3	-58.4	13.0	-42.1	-28.6	-21.3	37.6	66.5				
T4	0.6	1.4	4.8	2.4	0.3	0.6	4.9	9.8	1.14	1.03	0.85	7.5
	-50.3	-59.8	5.1	-51.6	-50.2	-29.4	25.7	195.6				
T5	2.6	3.6	5.5	5.6	0.3	0.9	6.1	9.1	0.9	1.1	0.87	6.1
	48.5	-25.5	30.1	-17.8	16.5	21.3	37.5	40.2				
T6	1.4	1.6	4.2	2.8	0.2	0.4	3.8	4.8	0.95	0.91	0.99	5.6
	64.1	-57.9	-14.0	-51.4	-46.8	-38.2	-4.7	11.8				
T7	1.7	1.8	4.2	2.8	0.2	0.5	4.4	81.0	0.81	1.05	0.92	4.7
	48.6	-34.7	18.7	-20.1	26.3	47.0	50.7	2723.1				
T8	0.2	0.1	1.2	0.4	0.1	0.1	1.1	3.8	1.41	0.87	1.01	8.3
	-95.3	-94.0	-67.3	-92.2	-76.4	-86.1	-74.1	-46.7				
T10	1.3	0.4	1.5	1.0	0.1	0.2	1.0	149.0	0.59	0.69	1.3	5.8
	-56.4	-32.0	-37.8	-56.9	-34.6	-34.3	-34.5	357.7				

depositions were estimated using the ion concentrations in the nearby Morro Mejillones surface soil (Wang et al., 2014). For most ions, < 4% of ion deposition could be attributed to the local soil deposition, and ~10% K⁺ was originated from local soil. Therefore, the 159% increase in the soluble salts deposition rate cannot be explained by the increased soil flux during 2010–2011 (Wang et al., 2014). In the following discussion we have subtracted the amount of salts attributed to local soil to assess the interannual variations of other ion sources at T1.

The 2010–2011 deposition rates of major cations (Na⁺, K⁺, Mg²⁺ and Ca²⁺) at T1 were significantly higher than those during 2007–2009, which could, in part, be attributed to the interannual variabilities in sea-salt aerosols (SSA) deposition. SSAs were formed by entraining the seawater droplets into the atmosphere that were generated by bursting air bubbles or tearing off of wave crests. The SSA deposition rates were commonly estimated using the Na⁺ deposition rate (e.g., Li et al., 2018; Norman et al., 1999) for three reasons. First, it is the most abundant cation in seawater (1.08 wt%, Rees et al., 1978) thus a major component in the SSAs. Second, Na⁺ is biologically inactive and is not likely subject to post-depositional chemical losses in arid regions. Third, it has low concentrations in local surface soil (discussed above) and lack any major anthropogenic sources. Using Na⁺ concentrations, we suggest the SSA concentration had increased by 75% during 2010–2011 relative to during 2007–2009.

The deposition of SSA at T1 consists of both wet (precipitation and fog) and dry depositions. For any ion, the annual ion deposition rate is quantified by

$$\text{Ion deposition rate} = p_d C_p + f_d v_f C_f + 365 * v_d C_a \quad (1)$$

The first two terms in Eq. (1) are the wet deposition rate and the latter is the dry deposition rate. In Eq. (1), p_d is the annual precipitation depth (m), C_p is the molar concentration of a SSA ion in rain (mmol * m⁻³), f_d is the number of fog days per year, v_f is the fog deposition velocity (m/day), C_f is the concentration of a SSA ion in fog water (mmol/m³), v_d is the dry deposition velocity (m/day) and C_a is the concentration of a SSA ion in the atmosphere (mmol/m³). An increase in precipitation, fog deposition velocities, and/or SSA concentrations would result in an increase in annual ion deposition rates, therefore we evaluated any potential increase in these terms during 2010–2011 relative to 2007–2009.

Changes in the annual precipitation depth (p_d) was determined using archived data from ASA (Andres Sabella Airport, NOAA Climate Data Online Database, 2018) station, located ~30 km south of the T1 site (Fig. 1). Annual precipitation depth at ASA was 1.0 mm/yr during 2007–2009 and 4.3 mm/yr during 2010–2011. The contribution of

precipitation to total deposition, however, was small. Assuming the precipitation contains 20 ppm Na⁺, an upper limit for Na⁺ concentrations in coastal rain (Brecciaroli et al., 2012), the precipitation only contributed 3.3 mmol/m²/yr of Na⁺ during 2010–2011 (8% of total Na⁺ deposition) and 0.5 mmol/m²/yr of Na⁺ during 2007–2009 (2% of total Na⁺ deposition). This was a net increase in Na⁺ deposition of only 2.8 mmol/m²/yr, which could only account for 15% of the observed increase (75%) in the Na⁺ deposition rate.

Changes in annual fog water deposition depth ($f_d v_f$) was also determined using archived meteorology data collected at ASA. Fog deposition was estimated by assuming fog would form when the minimum daily temperature was lower than the daily dew point and v_f was the same in both study periods. Daily temperature minimums at T1 (T_{\min}) were estimated using the minimum temperatures at ASA (T_0), the altitude difference between T1 and ASA ($h = 0.454$ km), and the dry adiabatic lapse rate ($L = -9.8$ K/km): $T_{\min} = T_0 + h * L$. By comparing T_{\min} and the daily dew point, fog events likely occurred 186 days/yr during 2007–2009 and 176 days/yr during 2010–2011. Using an estimated fog deposition of 0.1 mm per event (Merriam, 1973), and measured fog water Na⁺ concentration of 5 ppm (Schemenauer et al., 1992), we estimated that the Na⁺ flux from fog deposition was 4.2 mmol/m²/yr during 2007–2009 and 3.8 mmol/m²/yr during 2010–2011. This resulted in a 5% decrease, also cannot explain the observed 75% increase in SSA deposition in 2010–2011.

The higher SSA deposition at T1 may be due to an increased SSA dry deposition flux ($v_d * C_a$). The dry deposition velocity (v_d) of SSA deposition was often treated as a constant (Seinfeld et al., 1998; Tedeschi et al., 2017) since most SSA masses are in the large particle fraction (Liang et al., 2016; McDonald et al., 1982). Therefore, the changes in SSA should be mainly due to changes in SSA concentrations (C_a), which were strongly affected by wind speed (Jaeglé et al., 2011; Kishcha et al., 2011; Lewis and Schwartz, 2004; Li et al., 2018; Mårtensson et al., 2003; McDonald et al., 1982; O'dowd et al., 2007; Zakey et al., 2008). In the open ocean, SSA concentration is positively correlated to the wind speed. For example, Dror et al. (2018) observed a linear relationship between annual average wind speed and SSA concentration at South Pacific Ocean, showing a 0.4 m/s increase in wind speed would increase SSA concentration by ~10%. Using the wave height data (discussed above), which corresponding to an average wind speed increase of ~0.5 m/s in the 2010–2011 relative to 2007–2009, we suggested that the average SSA concentration in the open ocean during 2010–2011 should be 10% - 20% higher than during 2007–2009. While significant, this predicted increase was still significantly lower than our observed 75% increase at T1.

Unlike open ocean, the SSA production at coastal regions was also affected by the depth and topography of the sea floor (Lewis and Schwartz, 2004). As a result, the effect of wind speed on the concentrations of SSAs was no longer a simple linear relationship (Lewandowska and Falkowska, 2013). Exponential relationships between the wind speed and SSA concentrations had been observed along coastal areas (McDonald et al., 1982; Lewandowska and Falkowska, 2013). McDonald et al. (1982) suggested that an increase in wind speed from 3.4 m/s to 10 m/s could increase the SSA concentration by 6.7 times along the coast. Using the data in McDonald et al. (1982) and assuming SSA concentration increases exponentially with increasing wind speed, we estimated that 0.5 m/s increase in coastal wind speed could increase the SSA concentration by 15.2%. Lewandowska and Falkowska (2013) also noted an exponential increase of SSA concentration (i.e., Na^+ concentration) with increased wind speed (v) along coastal zones in southern Baltic Sea: $[\text{Na}^+] = 0.3 * e^{0.55*v}$ when $v > 7$ m/s and $[\text{Na}^+] = 4.3 * e^{0.30*v}$ when $v < 7$ m/s and $v > 5$ m/s. Using these equations, we calculated that an increase in wind speed of 0.5 m/s would result in 16–32% increase of SSA flux. The combination of above factors (15% increase of SSA from wet deposition, 10%–20% increase of SSA produced in the open ocean and 16–32% increase of SSA produced on the coast) still cannot fully account for the observed 75% increase in our sampling period, indicating other factors, i.e., strong wind events from the ocean, were important but unaccounted. Future study should use more sophisticated models to better quantify the emission of SSAs in the coastal areas (e.g., Callaghan, 2013; Demoisson et al., 2013) but it is beyond the scope of our work.

Non-sea-salt (NSS) soluble salts also contributed to the deposition of some inorganic ions at T1. The EFs of SO_4^{2-} , K^+ and Ca^{2+} were higher than 1, indicating extra sources of these ions other than SSAs at T1 (Table 2 and Fig. 4). Additionally, since SSAs contain little NO_3^- (Rees et al., 1978), the observed NO_3^- at T1 was also originated from NSS sources. While NSS-SO_4^{2-} and NO_3^- were mainly produced by atmospheric oxidation of NO_x and SO_2 gases (see detailed discussions below), NSS-K^+ and NSS-Ca^{2+} were likely directly emitted during several processes, including biomass burning, anthropogenic emissions and marine biogenic activities.

The NSS-K^+ deposition rate was calculated ($\text{NSS-K}^+ = [\text{K}^+]_{\text{T1}} - [\text{Na}^+]_{\text{T1}} \times (\text{K}^+/\text{Na}^+)_{\text{seawater}}$, where $(\text{K}^+/\text{Na}^+)_{\text{seawater}} = 0.0218$, Rees et al., 1978) to be 0.15 mmol/m²/yr during 2010–2011, decreased by ~63% compared to during 2007–2009 (0.41 mmol/m²/yr). The origins of NSS-K^+ at T1 were possibly forest biomass burning in central Chile and anthropogenic emissions (Fig. 4). Forest biomass burning in central Chile could be a major source of NSS-K^+ deposition (Bañales-Seguel et al., 2018; Pachon et al., 2013). The NSS-K^+ in aerosols (~40 ng/m³) at Papos, a small coastal town ~150 km away from Antofagasta, was suggested to be mainly originated from biomass burning (Chand et al., 2010). Meantime, anthropogenic emissions, especially coal burning, could be a potential NSS-K^+ source. Coal burning ash was suggested to contain 0.19% wt. to 0.71% wt. K^+ (Zhang et al., 2018), which could account for some of the K^+ deposition at T1 but was difficult to quantify. The number of forest fires in Chile had decreased from 6092 events per year during 2007–2009 to 4511 events per year during 2010–2011 (National

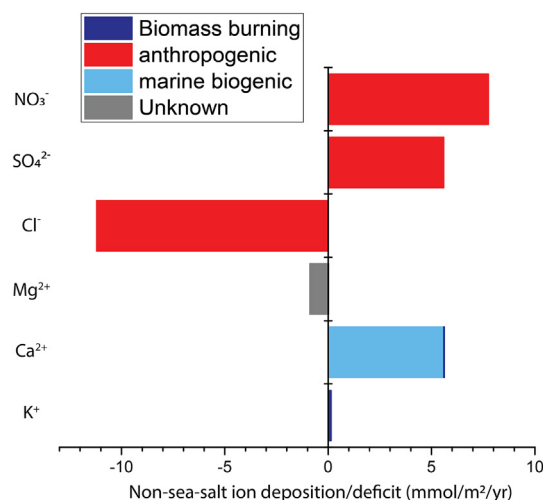


Fig. 4. NSS ions depositions (or SSA deficit) at T1. Positive values indicate non-sea-salt ion input ($\text{EF} > 1$) and negative values indicate deficit from sea salt composition. Different colors represent different processes that might lead to SSA deficit or serve as non-sea-salt sources.

Forest Corporation in Chile, 2018, in Spanish), and the energy production rate at Edelnor Power Plant located ~10 km from T1 the had decreased by 12% from 2007 to 2009 to 2010–2011 (Global Energy Observatory, 2011). These suggested a decreased NSS-K^+ emissions during 2010–2011, in agreement with the observed lower NSS-K^+ deposition rate.

The NSS-Ca^{2+} increased by 58% from 3.6 mmol/m²/yr during 2007–2009 to 5.6 mmol/m²/yr during 2010–2011. Using the emission factors of K^+ (0.29 g/kg) and Ca^{2+} (0.085 g/kg) during biomass burning (Akagi et al., 2011) and assuming all NSS-K^+ at T1 was originated from biomass burning, the maximum contribution of biomass burning NSS-Ca^{2+} was calculated to be 0.044 mmol/m²/yr. This small contribution was corresponding to 1.2% of total NSS-Ca^{2+} , suggesting biomass burning was not an important NSS-Ca^{2+} source (Fig. 4). Also, the NSS-Ca^{2+} was not likely derived from the entrainment of gypsum minerals because the nearest gypsum-rich salt playas existed > 80 km away from T1 and on the east side of the Coastal Range (Rech et al., 2003; Stoertz and Ericksen, 2009; Wang et al., 2014) from which the gypsum transportation should be substantially blocked. Therefore, we suggest marine CaCO_3 input from the microorganisms with calcified shells on the surface layer of the ocean might be the major source of NSS-Ca^{2+} (Fitzgerald, 1991; Hardy, 1982; MacIntyre, 1974; Wang et al., 2014). Although CaCO_3 aerosols were less soluble in water, they could form $\text{Ca}(\text{NO}_3)_2$ or CaSO_4 with soluble Ca^{2+} ions via acid displacement reactions in the atmosphere (see discussion below). Additionally, since marine biogenic CaCO_3 particles would be entrained into the atmosphere similar to SSAs, their variation in deposition rates should also be similar: the observed 58% increase in NSS-Ca^{2+} was in general agreement with the 75% increase in SSAs, again supporting our hypothesis that NSS-Ca^{2+} was probably marine biogenically originated.

The Mg^{2+} deposition rate was 3.8 mmol/m²/yr during 2010–2011, slightly depleted relative to seawater ($\text{EF}_{\text{Mg}} = 0.8$), and the Mg^{2+} deficit (0.9 mmol/m²/yr) decreased by 41% compared to during 2007–2009 (1.5 mmol/m²/yr, $\text{EF}_{\text{Mg}} = 0.5$, Fig. 4). Biomass burning could be a potential NSS-Mg^{2+} source and was calculated (similar to biomass burning Ca^{2+}) to be ~0.02 mmol/m²/yr. However, a depletion of Mg^{2+} relative to SSAs was observed, which was also previously observed during 2007–2009 and attributed to the formation of MgCO_3 and $\text{Mg}(\text{OH})_2$ inside the dust collection pan during fog events (Wang et al., 2014). Alternatively, the formation of Mg complexes with lipids, fatty acids and saccharides during the formation of SSAs (Jayarathne et al., 2016) might also resulted in the observed Mg^{2+} depletion. These

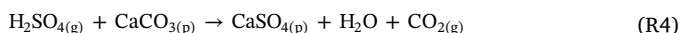
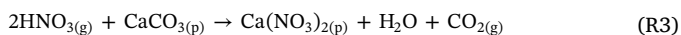
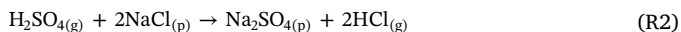
Table 2

Enrichment factors (EF) of each ion at T1.

Ion	EF
Na^+	1.00
K^+	1.17
Mg^{2+}	0.81
Ca^{2+}	7.26
Cl^-	0.76
SO_4^{2-}	4.14

Mg complexes were less soluble (or insoluble) due to their high molecular weight, thus some Mg might not be dissolved and were removed during the filtration, resulting in a lower dissolved Mg concentration relative to seawater.

The Cl^- deposition rate during 2010–2011 also increased relative to during 2007–2009 because of a higher SSA flux, but Cl^- was very depleted relative to seawater ($\text{EF}_{\text{Cl}^-} = 0.76$, Fig. 4). This chloride deficit was commonly observed in marine aerosols (Kerminen et al., 1998; Laskin et al., 2012; McInnes et al., 1994; Wang et al., 2014) and was due to the loss of Cl^- (and CO_3^{2-}) in aerosols via acid displacement reactions (Ayers et al., 1999; Metzger et al., 2006; Newberg et al., 2005):



Assuming SSA was the sole source of Cl^- at T1, the Cl^- deficit was calculated to be $11.2 \text{ mmol/m}^2/\text{yr}$, significantly less than the $17.9 \text{ mmol/m}^2/\text{yr}$ deficit during 2007–2009. This may be because CO_3^{2-} is kinetically and thermodynamically favorable to be displaced by HNO_3 or H_2SO_4 relative to Cl^- (Clarke and Karani, 1992). Assuming that CO_3^{2-} is present as CaCO_3 then the amount of CO_3^{2-} displaced should be equal to the amount of NSS-Ca^{2+} , i.e. $5.6 \text{ mmol/m}^2/\text{yr}$. The total negative charge deficit from Cl^- ($11.2 \text{ mmol/m}^2/\text{yr}$) and CO_3^{2-} ($5.6 \text{ mmol/m}^2/\text{yr}$) in milliequivalents (meq) was $11.2 + 5.6 \times 2 = 22.4 \text{ meq/m}^2/\text{yr}$. This is close to the total amount of NO_3^- ($5.6 \text{ meq/m}^2/\text{yr}$) and NSS-SO_4^{2-} ($7.8 \times 2 = 15.6 \text{ meq/m}^2/\text{yr}$) measured at T1.

The deposition of NO_3^- at T1 must be largely originated from anthropogenic N emissions and any interannual variation must be due to a change in N emissions (Alexander et al., 2009; Fitzgerald, 1991). The deposition rate of NO_3^- at T1 during 2010–2011 was $5.6 \text{ mmol/m}^2/\text{yr}$, a $\sim 61\%$ increase compared to during 2007–2009 (Wang et al., 2014), which should be attributed to an increased local NO_x emission (Galloway, 1985; Galloway et al., 1996). In November 2010 a new nitric acid plant was built near the city of Mejillones (Panna 4, Enaex S.A., Fig. 1), which was only 10 to 15 km away from T1 (Enaex Memoria Annual, 2011). Nitric acid plants emitted NO_x , N_2O and trace amounts of HNO_3 mist (Wood and Cowie, 2004), which could significantly increase local deposition rate of NO_3^- (Kumar et al., 2005; Schindler et al., 2006). This extra emission occurred in 14 of our 24-month sampling period (Nov. 2010 to Dec. 2011). Assuming the NO_3^- deposition rate in the first 10 months was the same as the 2007–2009 value, then the NO_3^- deposition rate due to the nitric acid plant could be as high as $7.1 \text{ mmol/m}^2/\text{yr}$, twice the NO_3^- deposition rate of 2007–2009. This increase was supported by the calculated HNO_3 emission from the plant that was calculated from the annual yield (800,000 tons/yr, Panna 4, Enaex S.A.; Enaex Memoria Annual, 2011, in Spanish) and the estimated NO_x emission factors ranging from 0.5 to 3 kg/ton (Cheremisnoff, 2016) by assuming the emitted HNO_3 were evenly spread within a 50 km radius. The HNO_3 deposition due to the plant ranged from 0.81 to $4.85 \text{ mmol/m}^2/\text{yr}$, consistent with the observed increase of $3.6 \text{ mmol/m}^2/\text{yr}$.

Both SS-SO_4^{2-} and NSS-SO_4^{2-} were important sulfate sources at T1. The SS-SO_4^{2-} deposition rate was $2.5 \text{ mmol/m}^2/\text{yr}$, and the NSS-SO_4^{2-} deposition rate ($7.9 \text{ mmol/m}^2/\text{yr}$) accounted for 76% of total SO_4^{2-} deposition rate at T1 during 2010–2011, similar to that of $8.1 \text{ mmol/m}^2/\text{yr}$ in 2007–2009. The NSS-SO_4^{2-} at T1, accounting for 74% of total Cl^- and CO_3^{2-} deficit, was also suggested to directly impact the number of cloud condensation nuclei (Lana et al., 2011; Li et al., 2018), and therefore, was important to understand its sources. Volcanic sources were ignored because of there was no nearby volcanic

eruptions during the sampling period. Therefore, NSS-SO_4^{2-} were mainly sourced from oxidation of SO_2 , which was either directly emitted from anthropogenic activities, or formed from oxidation of dimethyl sulfide (DMS) produced during marine biological processes (Li et al., 2018).

$\delta^{34}\text{S}_{\text{sulfate}}$ values were used to evaluate the relative contribution of anthropogenic and biogenic emissions to the NSS-SO_4^{2-} deposition rate. A two-component isotope mixing model was first used to evaluate the $\delta^{34}\text{S}$ of NSS-SO_4^{2-} ($\delta^{34}\text{S}_{\text{NSS}}$):

$$f_{\text{SS}} \delta^{34}\text{S}_{\text{SS}} + f_{\text{NSS}} \delta^{34}\text{S}_{\text{NSS}} = \delta^{34}\text{S}_{\text{T1}} \quad \text{Eq. 1}$$

$$f_{\text{SS}} + f_{\text{NSS}} = 1 \quad \text{Eq. 2}$$

where f_{SS} and f_{NSS} are the mole fractions of SS-SO_4^{2-} (0.24) and NSS-SO_4^{2-} (0.76), respectively; the $\delta^{34}\text{S}$ value of SS-SO_4^{2-} ($\delta^{34}\text{S}_{\text{SS}}$) is $21.0 \pm 0.1\%$ (Rees et al., 1978), and the measured $\delta^{34}\text{S}_{\text{sulfate}}$ value at T1 ($\delta^{34}\text{S}_{\text{T1}}$) is 4.0‰. This resulted in the $\delta^{34}\text{S}_{\text{NSS}}$ of -1.4% . Sulfate derived from anthropogenic coal burning had $\delta^{34}\text{S}$ values ranging from -3% to $+3\%$ (Norman et al., 1999), while biogenic DMS-derived SO_4^{2-} had the $\delta^{34}\text{S}$ values of $\sim +18\%$ (Sanusi et al., 2006; Patris et al., 2007). The calculated $\delta^{34}\text{S}_{\text{NSS}}$ of -1.4% suggested that regional anthropogenic SO_2 emissions (mostly coal burning at Edelnor Power Plant located $\sim 10 \text{ km}$ from T1) should be the dominant NSS-SO_4^{2-} source at T1: the contribution of anthropogenic emission was at least 92% ($\sim 7.3 \text{ mmol/m}^2/\text{yr}$) using the lower limit of anthropogenic $\delta^{34}\text{S}$ value (-3%) and could be as high as 100% ($\sim 7.9 \text{ mmol/m}^2/\text{yr}$). Anthropogenic sulfate deposition rate at T1 were previously estimated by Wang et al. (2014) using the inventory calculations, which suggested a range of $3.1 \text{ mmol/m}^2/\text{yr}$ to $5.8 \text{ mmol/m}^2/\text{yr}$, lower than our estimation. This discrepancy could be attributed to two possibilities. The first possibility was that the anthropogenic emissions during our sampling period had increased since the 2007–2009 period, possibly due to significantly higher SO_2 emissions at the Edelnor power plant. However, the energy production rate of the Edelnor power plant had decreased by 12% from 2007 to 2009 to 2010–2011 (Global Energy Observatory, 2011), and the SO_2 emission was unlikely to increase considering the anthropogenic S emission was usually proportional to the energy production in power plants. Alternatively, we suggest the flux calculation using emission inventory may underestimate the NSS-SO_4^{2-} deposition. Wang et al. (2014) calculated the SO_2 flux at T1 by assuming the emitted SO_2 was evenly distributed in a circle area with radius of 180–216 km, which was likely to underestimate the SO_4^{2-} deposition rate at T1 since T1 was only 10 km from the power plant.

The $\delta^{34}\text{S}_{\text{T1}}$ was significantly lower than the $\delta^{34}\text{S}$ of sulfate extracted from surface soil samples (Fig. 5) along a 50 km long west-east transect starting near Antofagasta by Rech et al. (2003). Sulfate in soils located $\sim 30 \text{ km}$ to the south of T1 site had $\delta^{34}\text{S}_{\text{sulfate}}$ values of $+15\%$ – $+18\%$, which were attributed to SS-SO_4^{2-} being the main source of soil sulfate near the coast. Our data suggested that anthropogenic sulfate

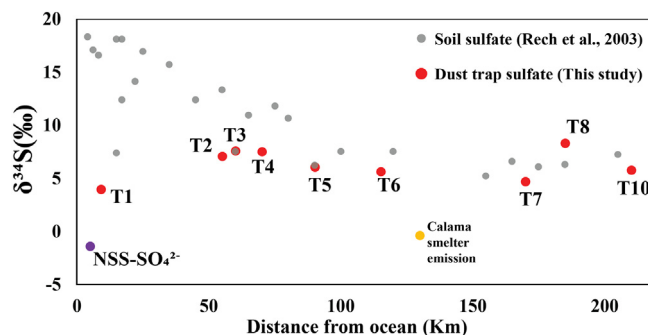


Fig. 5. $\delta^{34}\text{S}_{\text{sulfate}}$ values of atmospheric depositions at T1–T10 (red dots) comparing with $\delta^{34}\text{S}_{\text{sulfate}}$ values of nearby soil gypsum in Rech et al. (2003). (For interpretation of the references to color in this figure legend, the reader is referred to the web version of this article.)

depositions have recently dwarfed natural SO_4^{2-} deposition along the coast and is a further evidence of the Anthropocene (Capaldo et al., 1999; Crutzen, 2002; Li et al., 2018; Wadleigh, 2004).

4.2. Inland sites T2–T8

The 2010–2011 deposition data confirmed that the atmospheric depositions at T2 to T8 sites were likely controlled by local entrainment of insoluble dust and soluble salts as suggested by (Wang et al., 2014). Oceanic inputs at our inland sites were small because of fast settlement of large particles and efficient blocking by the Coastal Range (Wang et al., 2014; Rech et al., 2003), evidenced by the fact that the deposition rate of Na^+ at T2 was 90% lower than T1. Similarly, the material from the Andes was also unlikely to be transported to the inland sites for several reasons. First, the deposition rates of salts at the Andean site (T10, see discussion in Section 4.3) were much lower than the inland site traps, indicating very limited input from the Andean to the Atacama. Secondly, due to the daytime upslope air flow caused by the fast heating of the Andean west slopes, namely the “Andean pump effect” (Rutllant et al., 2013), the seaward air mass movement should be low and not conducive to the inland transportation of Andean inputs. Instead, the depositions at these inland sites were more likely derived from local entrainments of surface soil and anthropogenic emissions.

Insoluble dust deposition at the inland sites showed significant variations between the two sampling periods (50%–100% increase at T2–T6 sites, 46% decrease at T8 site, and 27 times increase at T7), which was caused by a combination of increased wind speed and anthropogenic activities. Significant spatial variations among different sites (3.8–80.9 g/m²/yr) were again observed. Since all the traps were set in the open field with small geomorphological variations among the locations of traps (Wang et al., 2014), these spatial variations were unlikely caused by biased sampling but reflected the average atmospheric depositions of the region. However, all the sites except for T8 (discussed below) displayed significant increases in insoluble dust deposition rates during 2010–2011, which can be attributed to a combination of higher average wind speed (Watts et al., 2017) and enhanced anthropogenic activities. The archived wind speed data at Calama site (Fig. 1, NOAA Climate Data Online Database, 2018) showed that the average wind speed during 2010–2011 (14.9 ± 2.0 m/s, $n = 630$) was statistically significantly higher ($p < 0.05$) than those of 2007–2009 (14.6 ± 2.0 m/s, $n = 811$). This increased wind speed can at least partially explain the general increasing trend in insoluble dust deposition at T2–T6, similar to the increased insoluble dust deposition at the coastal site (T1). Similar interannual variations have also been observed at several desert sites in California (Reheis, 1997; Reheis and Kihl, 1995), probably owing to the susceptibility of surface soil to local entrainment in arid environments. Meanwhile, the huge increase in insoluble dust deposition at T7 (27 times increase) was possibly caused by nearby anthropogenic activities. The satellite images near T7 (Fig. 6A, B) suggested that a major new mine located ~60 km SW from T7 came into operation between 2007 and 2011. Meantime, the size of another open-pit gravel mine located 10 km from T7 expanded significantly from 2007 to 2011 (Fig. 6C, D). These mining activities could significantly increase local soil entrainment and insoluble dust deposition rate at T7.

The soluble salts at T2–T8 were mainly in the forms of $\text{Na}(\text{Cl}, \text{NO}_3)$ and CaSO_4 with the molar ratios of both $\text{Na}^+(\text{Cl}^- + \text{NO}_3^-)$ and $\text{Ca}^{2+}/\text{SO}_4^{2-}$ close to 1 (except for T8, see discussion below). The $\text{Ca}^{2+}/\text{SO}_4^{2-}$ molar ratios in these traps of ~1 (i.e. 0.87 to 1.10) suggested that CaSO_4 was mostly sourced from the widespread gypsum minerals in local surface soil (Ericksen, 1981; Rech et al., 2003). Na^+ and Cl^- were likely originated from chloride deposits in the nearby salt playas. For example, the Salar de Pampa Blanca located only 7.5 km from T5 (Stoertz and Ericksen, 2009) likely contributed to the highest deposition rates of Na^+ and Cl^- at T5 among the seven inland sites. The NO_3^- deposition at T2–T7 (1.4 to 3.6 mmol/m²/yr) can originate from both

anthropogenic NO_x emissions and local soil entrainment (Michalski et al., 2003). The Cl^-/Na^+ ratio at T2–T7 averaged at 0.42 ± 0.15 , close to the average Cl^-/Na^+ ratio (0.43) in the Atacama soil (Grossling and Ericksen, 1971; Michalski et al., 2004), supporting that most Na^+ and Cl^- should be originated from local soil and salt playas. In 2010–2011, the deposition rates of CaSO_4 at T2 and T6 slightly decreased by 5.7%–9.4% while other traps showed increases of 15.4%–34.7%; the Na^+ deposition rate at T2 increased by 2.7% and other traps showed decreased depositions by 17.8%–51.6%. This overall increased CaSO_4 deposition and decreased $\text{Na}(\text{Cl}, \text{NO}_3)$ deposition can also be explained by the increased wind during 2010–2011. Most Atacama soil had a well-developed gypsum crust on the surface, while the nitrate and chloride were usually observed beneath the surface layer (Wang et al., 2014). As a result, stronger wind would result in more entrainment from the surface layer and less entrainment from the deeper soil layers. However, these ratios were significantly higher than the Cl^-/Na^+ ratios observed in 2007–2009 (0.25 ± 0.07), where (Wang et al., 2014) suggested that significant acidic displacement reaction had occurred. This higher ratio, along with lower NO_3^- deposition rate in 2010–2011 (38% lower than 2007–2009), suggested weaker acidic displacement during our sampling period. This may at least partially be attributed to a drier climate during 2010–2011 since the acidic displacement reaction will be greatly inhibited at a lower relative humidity (RH) (Laskin et al., 2012): at the Calama site (near T6 & T7): the average RH during 2007–2009 was 33.5% while the average RH during 2010–2011 was 27.6%.

The $\delta^{34}\text{S}_{\text{sulfate}}$ at T2–T4 ranged from 7.1‰ to 7.6‰, similar to those of gypsum minerals from nearby surface soil observed in Rech et al. (2003, Fig. 5), corroborating the major source of sulfate in these inland dust traps was local soil entrainment. A decrease in $\delta^{34}\text{S}_{\text{sulfate}}$ from 7.1‰ to 4.7‰ was observed at T5–T7, possibly due to the mixing of gypsum mineral and secondary sulfate oxidized from SO_2 emitted from Chuquicamata smelter near T7, where the $\delta^{34}\text{S}$ of sulfide minerals at this mine sites ranged from -4.7‰ to $+4.0\text{‰}$ (U.S. Geological Survey, 2005). If we assume the $\delta^{34}\text{S}$ value of sulfate in local soil was 7.4‰ (average value of T2–T4), and the secondary sulfate from Chuquicamata smelters had a $\delta^{34}\text{S}$ value of -0.4‰ , the contribution of sulfate from anthropogenic SO_2 at T5, T6, T7 would be 17%, 23% and 35%, respectively.

The decrease in both insoluble dust and soluble salts depositions at T8 during 2010–2011 may be attributed to a combination of lower atmospheric deposition and the loss of deposition sample during the sampling period. The insoluble dust flux at T8 had decreased by 47% in 2010–2011 while the soluble salts deposition had a much higher decrease of 80%, from 0.92 g/m²/yr (highest among T2–T8) during 2007–2009 to 0.18 g/m²/yr (lowest among T2–T8). We suggest these low values should at least partially be attributed to the loss of some insoluble dust and soluble salts by leaching during the sampling period. Two facts could support this hypothesis. First, Na^+ , Cl^- , and NO_3^- depositions had decreased by ~92–95% while Ca^{2+} and SO_4^{2-} decreased by only 67% and 74% (Fig. 3), and this discrepancy was likely resulted from leaching since $\text{Na}(\text{Cl}, \text{NO}_3)$ was more soluble and subject to leaching losses than CaSO_4 . Second, the $\delta^{34}\text{S}_{\text{sulfate}}$ at T8 showed the highest value of 8.3‰ among the inland sites (Fig. 5), significantly higher than at T7 (4.7‰) and adjacent surface soil (5.4‰, Rech et al., 2003). This is likely caused by the enrichment in $\delta^{34}\text{S}_{\text{sulfate}}$ during dissolution of gypsum minerals, with the equilibrium fractionation factor between solid and dissolved CaSO_4 of ~2‰ at 273 K (Van Driessche et al., 2016).

4.3. Andean site T10

The insoluble dust deposition rate (149.0 g/m²/yr) at T10 during 2010–2011 was the highest among all sites and increased by 3.6 times compared to that of 2007–2009 (Fig. 2), probably due to the interannual variations in precipitation. T10 was located at a valley on the

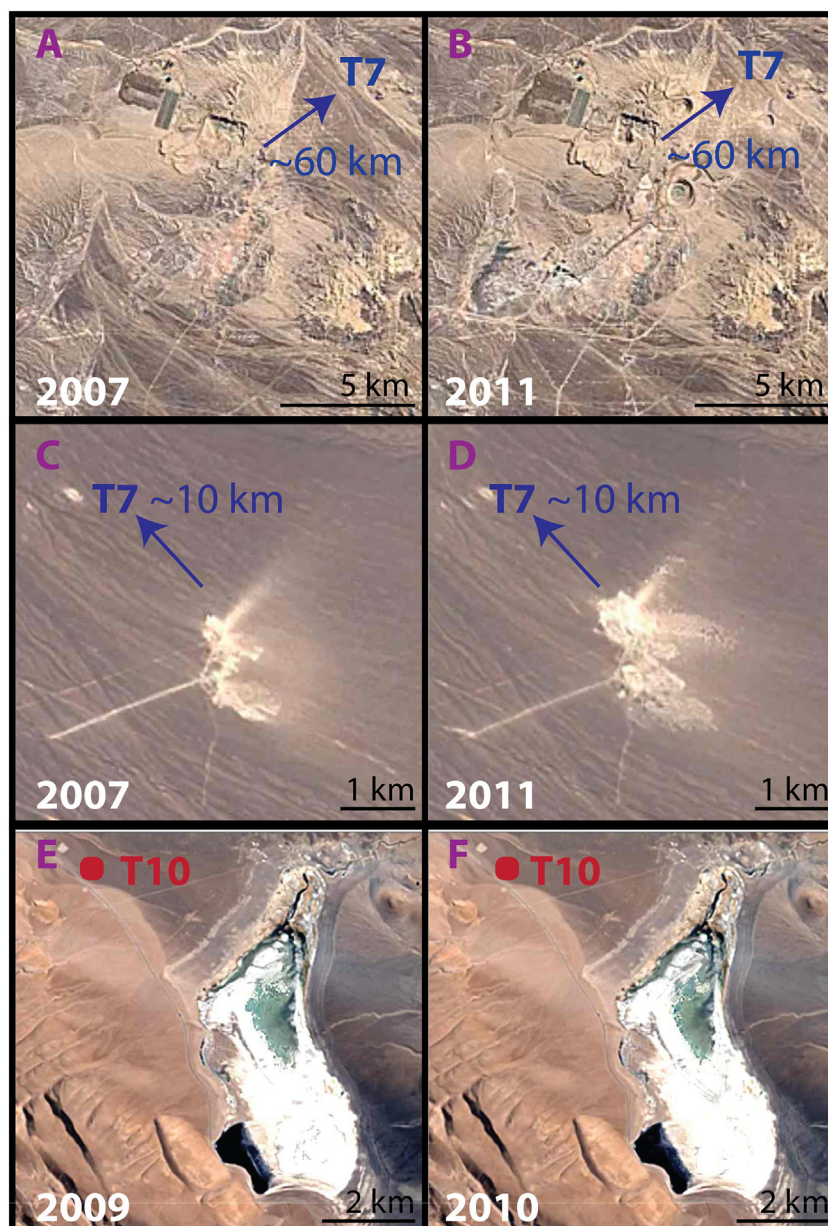


Fig. 6. Google Time Lapse images for 3 locations near sampling sites: A, B: a mine site located ~60 km SW from T7; C, D: an open-pit mine located 10 km from T7; E, F: the lake next to T10.

Andean altiplano receiving significant amount of precipitation (MAP ~150 mm). The insoluble dust was likely from local soil entrainment by winds; hence its deposition rate would be strongly affected by both wind speed and precipitation. However, there was no wind speed or precipitation observation available near T10. We used the ERA-interim reanalysis data (Dee et al., 2011) to investigate the variations in wind speed. The modelled average wind speeds were 1.59 m/s during 2007–2009 and 1.61 m/s during 2010–2011, therefore it might not be able to account for the 3.6 times increase in insoluble dust flux. The precipitation during 2010–2011 likely decreased comparing to 2007–2009, since the size of local lakes located near T10 was observed to have decreased in December of 2010 (Fig. 6E, F) compared to that in January of 2009. This observation agreed with the occurrence of El Niño in 2009: El Niño has been linked to increased precipitation in the Andean area (Bozkurt et al., 2016; Mason and Goddard, 2001; Ropelewski and Halpert, 1989; Valdés-Pineda et al., 2016), and therefore the average precipitation during 2007–2009 (2 years of La Niña and 1 year of El Niño) was likely higher than that of 2010–2011 (2 years

of La Niña). The decreased precipitation at T10 could increase wind erosion and thus significantly increase the insoluble dust flux (Reheis and Kihl, 1995).

In contrast with T1–T8, the soluble salts depositions at T10 had decreased. This is because the soluble salts at T10 were mostly from wet deposition, mainly snow, as suggested by (Ginot et al., 2001; Houston, 2007; Wang et al., 2014). The dry deposition had little contribution to the total salt deposition at T10 because 1) concentrations of soluble ions in dust (local soil) near T10 were extremely low (0.0005 mmol/g Cl^- , 0.0004 mmol/g SO_4^{2-} and undetectable NO_3^- , Wang et al., 2014) thus the salt from dust only accounted for < 6% of total Cl^- and < 5% of total SO_4^{2-} ; 2) T10 was distant from both the ocean and anthropogenic activities, thus lacking SSAs or anthropogenic secondary aerosols. Meantime, wet deposition, especially snow deposition, played an important role in the salt deposition at T10 because snow could incorporate ions from a few reservoirs, such as NaCl and CaSO_4 from the salt lakes (e.g., Tara Lake, Wang et al., 2014) on the Andean plateau. In 2010–2011, the deposition rates of Na^+ , Cl^- , Ca^{2+} , SO_4^{2-} decreased

by 34% to 57% relative to 2007–2009, which should be attributed to the decreased precipitation at T10 during 2010–2011.

The $\delta^{34}\text{S}_{\text{sulfate}}$ at T10 was 5.8‰, close to the $\delta^{34}\text{S}$ value of gypsum at Tara Lake (5.2‰, Risacher et al., 2011), again supporting that the origin of sulfate deposition was local gypsum. Precipitations could incorporate some gypsum from nearby salt lakes and deposit back to the surface (Wang et al., 2014), the $\delta^{34}\text{S}$ value of which was also similar to the $\delta^{34}\text{S}$ values of soil gypsum (5.2–7.5‰) in the Atacama (Rech et al., 2003), further evidencing that the surface soil gypsum in the Atacama Desert was probably originated from local salt lakes. The salt-rich soil was either formed via subsurface chemical weathering processes (Rech et al., 2003), or other deeper soil development processes, such as groundwater flow (Cameron and Leybourne, 2005). The salts were then transported either directly by wind as insoluble dust across the Atacama Desert (T2–T8) or incorporated into precipitation (at T10) and transported within the Andes, then deposited onto the surface.

The NO_3^- deposition rate at T10 was 0.37 mmol/m²/yr during 2010–2011, slightly lower than 0.54 mmol/m²/yr during 2007–2009, which also could be due to the decrease in precipitation. These values are close to the NO_3^- deposition rate at the Torres del Paine National Park in southern Chile (0.36 mmol/m²/yr, Galloway et al., 1996), which is a remote coastal site with minor anthropogenic activities, suggesting minimal anthropogenic N emission at T10 (Wang et al., 2014). In remote areas, N could generally derive from soil emissions (nitrification and denitrification), lightning, lower stratosphere mixing and long-distance transportation of peroxyacetyl nitrate (PAN) at the top of troposphere (Crutzen, 1979; Galloway et al., 2004; Holland et al., 1999; Singh et al., 1985; Singh and Hanst, 1981). The 31% decrease of NO_3^- in 2010–2011 is similar to the decrease of Na^+ , Cl^- , Ca^{2+} , SO_4^{2-} depositions, indicating that these deposition rates were likely controlled by wet deposition.

5. Conclusions

In this work we investigated the sources, compositions and inter-annual variabilities of atmospheric depositions across the Atacama Desert. The nine dust trap sites across the Atacama Desert displayed significant spatial variations in atmospheric deposition because of their different geomorphological features and the characteristics sources at each site. The atmospheric deposition at coastal site T1 mainly consisted of local soil (as insoluble dust) and sea-salt aerosols (as soluble salts). NSS-SO_4^{2-} and NO_3^- at T1 were mainly originated from anthropogenic emissions, then entered particle phase via acidic displacement reaction. At inland sites T2–T8, the insoluble dust was from local soil entrainment and the soluble salts were likely originated from nearby salars and salt lakes. The insoluble dust deposition at the Andean site (T10) was also dominated by local soil but the soluble salts were mainly from wet depositions. The rate of atmospheric deposition (both insoluble dust and soluble salts) displays strong variations between the two sampling periods. At the coastal site T1, the deposition rates of both insoluble dust and salts during 2010–2011 had increased significantly comparing to during 2007–2009, due to higher wind speeds. Anthropogenic NO_3^- also had increased as a result of higher NO_x emissions from a newly built nitric acid plant near T1. At the inland sites T2–T8, the increased insoluble dust and gypsum depositions resulted from a windier and drier climate in the Atacama during 2010–2011. In the meantime, a drier climate at the Andean site (T10) likely had resulted in a higher insoluble dust deposition rate and a lower soluble salts deposition rate.

Our observation confirmed that the insoluble dust at all the sampling sites was mainly originated from local surface soil and weathered material. The salt depositions were strongly impacted by the ocean input in the coastal region, but in inland areas the erosions of local salars and salt lakes were more important. Shifted climate conditions (such as wind speed and precipitations) can impact the flux of both insoluble dust and soluble salts, and the dust fluxes were more easily to

be influenced than salt fluxes.

Anthropogenic activities impacted the atmospheric depositions across the Atacama in two ways. First, the open-pit mining activities greatly increased the dust flux at nearby areas, as suggested by the observed high dust flux at T7 during our sampling period. Second, anthropogenic SO_2 and NO_x formed sulfate and nitrate aerosols, which increased SO_4^{2-} and NO_3^- deposited in the Atacama Desert. Our isotopic evidence suggested that the SO_4^{2-} originated from smelters contributed up to 35% of total sulfate in nearby dust traps.

Acknowledgements

This work was supported by the National Science Foundation Grant (EAR 0922114) to GM. We thank Brenda Bowen, Ji-Hye Seo, Hao Luo, Mark Fisher and Jiayu Ren for their assistance in the lab and in the field. JL also thanks the fellowship funding support from Purdue Climate Change Research Center.

References

- Akagi, S.K., Yokelson, R.J., Wiedinmyer, C., Alvarado, M.J., Reid, J.S., Karl, T., Crouse, J.D., Wennberg, P.O., 2011. Emission factors for open and domestic biomass burning for use in atmospheric models. *Atmos. Chem. Phys.* 11, 4039–4072.
- Alexander, B., Hastings, M.G., Allman, D.J., Dachs, J., Thornton, J.A., Kunasek, S.A., 2009. Quantifying atmospheric nitrate formation pathways based on a global model of the oxygen isotopic composition ($\Delta^{17}\text{O}$) of atmospheric nitrate. *Atmos. Chem. Phys.* 9, 5043–5056.
- Álvarez, F., Reich, M., Snyder, G., Pérez-Fodich, A., Muramatsu, Y., Daniele, L., Fehn, U., 2016. Iodine budget in surface waters from Atacama: natural and anthropogenic iodine sources revealed by halogen geochemistry and iodine-129 isotopes. *Appl. Geochem.* 68, 53–63.
- Ayers, G.P., Gillett, R.W., Caaney, J.M., Dick, A.L., 1999. Chloride and bromide loss from Sea-Salt Particles in Southern Ocean Air. *J. Atmos. Chem.* 33, 299–319. <https://doi.org/10.1023/A:1006120205159>.
- Bañales-Seguel, C., De La Barrera, F., Salazar, A., 2018. An analysis of wildfire risk and historical occurrence for a Mediterranean biosphere reserve, Central Chile. *J. Environ. Eng. Landsc. Manag.* 26, 128–140.
- Bao, H., Jenkins, K.A., Khachatryan, M., Diaz, G.C., 2004. Different sulfate sources and their post-depositional migration in Atacama soils. *Earth Planet. Sci. Lett.* 224, 577–587. <https://doi.org/10.1016/j.epsl.2004.05.006>.
- Böhlke, J.K., Erickson, G.E., Revesz, K., 1997. Stable isotope evidence for an atmospheric origin of desert nitrate deposits in northern Chile and southern California, U.S.A. *Chem. Geol.* 136, 135–152. [https://doi.org/10.1016/S0009-2541\(96\)00124-6](https://doi.org/10.1016/S0009-2541(96)00124-6).
- Bozkurt, D., Rondanelli, R., Garreaud, R., Arriagada, A., 2016. Impact of warmer eastern tropical Pacific SST on the March 2015 Atacama floods. *Mon. Weather Rev.* 144, 4441–4460.
- Brecciaroli, G., Cocco, S., Agnelli, A., Courchesne, F., Corti, G., 2012. From rainfall to throughfall in a maritime vineyard. *Sci. Total Environ.* 438, 174–188.
- Callaghan, A.H., 2013. An improved whitecap timescale for sea spray aerosol production flux modeling using the discrete whitecap method. *J. Geophys. Res. Atmos.* 118, 9910–9997.
- Cameron, E.M., Leybourne, M.I., 2005. Relationship between groundwater chemistry and soil geochemical anomalies at the Spence copper porphyry deposit, Chile. *Geochemistry Explor. Environ. Anal.* 5, 135–145.
- Capaldo, K., Corbett, J.J., Kasibhatla, P., Fischbeck, P., Pandis, S.N., 1999. Effects of ship emissions on sulphur cycling and radiative climate forcing over the ocean. *Nature* 400, 743–746. <https://doi.org/10.1038/23438>.
- Catling, D.C., Claire, M.W., Zahnle, K.J., Quinn, R.C., Clark, B.C., Hecht, M.H., Kounaves, S., 2010. Atmospheric origins of perchlorate on Mars and in the Atacama. *J. Geophys. Res.* 115, E00E11. <https://doi.org/10.1029/2009JE003425>.
- Chand, D., Hegg, D.A., Wood, R., Shaw, G.E., Wallace, D., Covert, D.S., 2010. Source attribution of climatically important aerosol properties measured at Papos (Chile) during VOCALS. *Atmos. Chem. Phys.* 10, 10789–10801.
- Cheremisinoff, N., 2016. AP-42, compilation of air pollutant emission factors. *Pollut. Control Handb. Oil Gas Eng.* <https://doi.org/10.1002/9781119117896.ch6>.
- Clarke, J.D.A., 2005. Antiquity of Aridity in the Chilean Atacama Desert. <https://doi.org/10.1016/j.geomorph.2005.06.008>.
- Clarke, A.G., Karani, G.N., 1992. Characterisation of the carbonate content of atmospheric aerosols. *J. Atmos. Chem. Phys.* 14, 119–128.
- Cooke, R.U., Warren, A., 1973. *Geomorphology in Deserts*. Univ of California Press.
- Crutzen, P.J., 1979. The role of NO and NO₂ in the chemistry of the troposphere and stratosphere. *Annu. Rev. Earth Planet. Sci.* 7, 443–472.
- Crutzen, P.J., 2002. The “anthropocene.” *Journal de Physique IV (Proceedings) 1–5 EDP sciences*.
- Darwin, C., 1906. *The Voyage of the Beagle*. JM Dent & sons.
- Dee, D.P., Uppala, S.M., Simmons, A.J., Berrisford, P., Poli, P., Kobayashi, S., Andrae, U., Balsameda, M.A., Balsamo, G., Bauer, D.P., 2011. The ERA-Interim reanalysis: configuration and performance of the data assimilation system. *Q. J. R. Meteorol. Soc.* 137, 553–597.
- Demoisson, A., Tedeschi, G., Piazzola, J., 2013. A model for the atmospheric transport of

- sea-salt particles in coastal areas. *Atmos. Res.* 132, 144–153.
- Dror, T., Lehahn, Y., Altaratz, O., Koren, I., 2018. Temporal-scale analysis of environmental controls on sea spray aerosol production over the South Pacific Gyre. *Geophys. Res. Lett.* 45, 8637–8646.
- Edwards, H.G.M., Villar, S.E.J., Parnell, J., Cockell, C.S., Lee, P., 2005. Raman spectroscopic analysis of cyanobacterial gypsum halotrophs and relevance for sulfate deposits on Mars. *Analyst* 130, 917–923.
- Enaex Memoria Annual, 2011. http://www.enaex.com/wp-content/uploads/2015/07/Memoria_2011.pdf.
- Ericksen, G.E., 1981. Geology and Origin of the Chilean Nitrate Deposits. USGPO.
- Ericksen, G.E., 1983. The Chilean nitrate deposits: the origin of the Chilean nitrate deposits, which contain a unique group of saline minerals, has provoked lively discussion for more than 100 years. *Am. Sci.* 71, 366–374.
- Ewing, S.A., Sutter, B., Owen, J., Nishiizumi, K., Sharp, W., Cliff, S.S., Perry, K., Dietrich, W., McKay, C.P., Amundson, R., 2006. A threshold in soil formation at Earth's arid-hyperarid transition. *Geochim. Cosmochim. Acta* 70, 5293–5322. <https://doi.org/10.1016/j.gca.2006.08.020>.
- Ewing, S.A., Yang, W., DePaolo, D.J., Michalski, G., Kendall, C., Stewart, B.W., Thiemens, M., Amundson, R., 2008. Non-biological fractionation of stable Ca isotopes in soils of the Atacama Desert, Chile. *Geochim. Cosmochim. Acta* 72, 1096–1110. <https://doi.org/10.1016/j.gca.2007.10.029>.
- Fishbaugh, K.E., Poulet, F., Chevrier, V., Langevin, Y., Bibring, J., 2007. On the origin of gypsum in the Mars north polar region. *J. Geophys. Res. Planets* 112.
- Fitzgerald, J.W., 1991. Marine aerosols: a review. *Atmos. Environ. Part A. Gen. Top.* 25, 533–545. [https://doi.org/10.1016/0960-1686\(91\)90050-H](https://doi.org/10.1016/0960-1686(91)90050-H).
- Galloway, J.N., 1985. The deposition of sulfur and nitrogen from the remote atmosphere background paper. In: *The Biogeochemical Cycling of Sulfur and Nitrogen in the Remote Atmosphere*. Springer, pp. 143–175.
- Galloway, J.N., Keene, W.C., Likens, G.E., 1996. Processes controlling the composition of precipitation at a remote southern hemispheric location: Torres del Paine National Park, Chile. *J. Geophys. Res. Atmos.* 101, 6883–6897. <https://doi.org/10.1029/95JD03229>.
- Galloway, J.N., Dentener, F.J., Capone, D.G., Boyer, E.W., Howarth, R.W., Seitzinger, S.P., Asner, G.P., Cleveland, C.C., Green, P.A., Holland, E.A., Karl, D.M., Michaels, A.F., Porter, J.H., Townsend, A.R., Vosmart, C.J., 2004. Nitrogen cycles: past, present, and future. *Biogeochemistry* 70, 153–226. <https://doi.org/10.1007/s10533-004-0370-0>.
- Genot, P., Kull, C., Schwikowski, M., Schotterer, U., Gäggeler, H.W., 2001. Effects of postdepositional processes on snow composition of a subtropical glacier (Cerro Tapado, Chilean Andes). *J. Geophys. Res. Atmos.* 106, 32375–32386. <https://doi.org/10.1029/2000JD000071>.
- Global Energy Observatory, 2011. <http://globalenergyobservatory.org/geoid/44595>.
- Goudie, A.S., Middleton, N.J., 1992. The changing frequency of dust storms through time. *Clim. Chang.* 20, 197–225.
- Grossling, B.F., Ericksen, G.E., 1971. Computer studies of the composition of Chilean Nitrate ores: data reduction, basic statistics and correlation analysis. No. 71-138. US Geological Survey.
- Group, T.W., 1988. The WAM model—a third generation ocean wave prediction model. *J. Phys. Oceanogr.* 18, 1775–1810.
- Hardy, J.T., 1982. The sea surface microlayer: biology, chemistry and anthropogenic enrichment. *Prog. Oceanogr.* 11, 307–328.
- Hecht, M.H., Kounaves, S.P., Quinn, R.C., West, S.J., Young, S.M.M., Ming, D.W., Catling, D.C., Clark, B.C., Boynton, W.V., Hoffman, J., 2009. Detection of perchlorate and the soluble chemistry of martian soil at the Phoenix lander site. *Science* 325, 64–67 (80-).
- Holland, E.A., Dentener, F.J., Braswell, B.H., Sulzaman, J.M., 1999. Contemporary and pre-industrial global reactive nitrogen budgets. In: *New Perspectives on Nitrogen Cycling in the Temperate and Tropical Americas*. Springer, pp. 7–43.
- Houston, J., 2007. Recharge to groundwater in the Turi Basin, northern Chile: an evaluation based on tritium and chloride mass balance techniques. *J. Hydrol.* 334, 534–544. <https://doi.org/10.1016/j.jhydrol.2006.10.030>.
- Jaeglé, L., Quinn, P.K., Bates, T.S., Alexander, B., Lin, J.-T., 2011. Global distribution of sea salt aerosols: new constraints from in situ and remote sensing observations. *Atmos. Chem. Phys.* 11, 3137–3157.
- Jayarathne, T., Sultana, C.M., Lee, C., Malfatti, F., Cox, J.L., Pendergraft, M.A., Moore, K.A., Azam, F., Tivanski, A.V., Cappa, C.D., 2016. Enrichment of saccharides and divalent cations in sea spray aerosol during two phytoplankton blooms. *Environ. Sci. Technol.* 50, 11511–11520.
- Kerminen, V.-M., Teinilä, K., Hillamo, R., Pakkanen, T., 1998. Substitution of chloride in sea-salt particles by inorganic and organic anions. *J. Aerosol Sci.* 29, 929–942.
- Kishcha, P., Starobinets, B., Bozzano, R., Pensieri, S., Canepa, E., Nickovic, S., di Sarra, A., Udisti, R., Becagli, S., Alpert, P., 2011. Sea-salt aerosol forecasts compared with wave height and sea-salt measurements in the open sea. In: *Air Pollution Modeling and Its Application XXI*. Springer, pp. 299–303.
- Kounaves, S.P., Carrier, B.L., O'Neil, G.D., Stroble, S.T., Claire, M.W., 2014. Evidence of martian perchlorate, chlorate, and nitrate in Mars meteorite EETA79001: implications for oxidants and organics. *Icarus* 229, 206–213.
- Kumar, R., Rani, A., Kumari, K.M., Srivastava, S.S., 2005. Atmospheric dry deposition to marble and red stone. *J. Atmos. Chem.* 50, 243–261.
- Lana, A., Bell, T.G., Simó, R., Vallina, S.M., Ballabrera-Poy, J., Kettle, A.J., Dachs, J., Bopp, L., Saltzman, E.S., Stefels, J., Johnson, J.E., Liss, P.S., 2011. An updated climatology of surface dimethylsulfide concentrations and emission fluxes in the global ocean. *Glob. Biogeochem. Cycles*. <https://doi.org/10.1029/2010GB003850>.
- Laskin, A., Moffet, R.C., Gilles, M.K., Fast, J.D., Zaveri, R.A., Wang, B., Nigge, P., Shuthanandan, J., 2012. Tropospheric chemistry of internally mixed sea salt and organic particles: surprising reactivity of NaCl with weak organic acids. *J. Geophys. Res. Atmos.* 117.
- Lewandowska, A.U., Falkowska, L.M., 2013. Sea salt in aerosols over the southern Baltic. Part 1. The generation and transportation of marine particles. *Oceanologia* 55, 279–298.
- Lewis, E.R., Schwartz, S.E., 2004. Sea Salt Aerosol Production: Mechanisms, Methods, Measurements, and Models—a Critical Review. American geophysical union.
- Li, J., Michalski, G., Davy, P., Harvey, M., Katzman, T., Wilkins, B., 2018. Investigating Source Contributions of Size-Aggregated Aerosols Collected in Southern Ocean and Baring Head, New Zealand Using Sulfur Isotopes. *Geophys. Res. Lett.* 45 (8), 3717–3727.
- Liang, T., Chamecki, M., Yu, X., 2016. Sea salt aerosol deposition in the coastal zone: a large eddy simulation study. *Atmos. Res.* 180, 119–127.
- MacIntyre, F., 1974. Chemical fractionation and sea-surface microlayer processes. *sea* 5, 245–299.
- Mårtensson, M., Nilsson, E.D., De Leeuw, G., Cohen, L.H., Hansson, H.C., 2003. Laboratory simulations of the primary marine aerosol generated by bubble bursting. *JGR-Atmospheres* 108.
- Mason, S.J., Goddard, L., 2001. Probabilistic precipitation anomalies associated with ENSO. *Bull. Am. Meteorol. Soc.* 82, 619–638.
- McDonald, R.L., Unni, C.K., Duce, R.A., 1982. Estimation of atmospheric sea salt dry deposition: wind speed and particle size dependence. *J. Geophys. Res. Ocean.* 87, 1246–1250.
- McFadden, L.D., Wells, S.G., Jercinovich, M.J., 1987. Influences of eolian and pedogenic processes on the origin and evolution of desert pavements. *Geology* 15, 504–508.
- McInnes, L.M., Covert, D.S., Quinn, P.K., Germani, M.S., 1994. Measurements of chloride depletion and sulfur enrichment in individual sea-salt particles collected from the remote marine boundary layer. *J. Geophys. Res. Atmos.* 99, 8257–8268.
- Merriam, R.A., 1973. Fog drip from artificial leaves in a fog wind tunnel. *Water Resour. Res.* 9, 1591–1598.
- Metzger, S., Mihalopoulos, N., Lelieveld, J., 2006. Importance of mineral cations and organics in gas-aerosol partitioning of reactive nitrogen compounds: case study based on MINOS results. *Atmos. Chem. Phys. Atmos. Chem. Phys.* 6, 2549–2567.
- Michalski, G., Scott, Z., Kabling, M., Thiemens, M.H., 2003. First measurements and modeling of $\Delta^{17}\text{O}$ in atmospheric nitrate. *Geophys. Res. Lett.* 30. <https://doi.org/10.1029/2003GL017015>.
- Michalski, G., Böhlke, J.K.K., Thiemens, M., 2004. Long term atmospheric deposition as the source of nitrate and other salts in the Atacama Desert, Chile: new evidence from mass-independent oxygen isotopic compositions. *Geochim. Cosmochim. Acta* 68, 4023–4038. <https://doi.org/10.1016/j.gca.2004.04.009>.
- National Data Buoy Center, 2018. https://www.ndbc.noaa.gov/station_page.php?station=32012.
- National Forest Corporation in Chile, 2018. <http://www.conaf.cl/incendios-forestales/incendios-forestales-en-chile/estadisticas-historicas/>.
- National Weather Service, 2015. http://origin.cpc.ncep.noaa.gov/products/analysis_monitoring/ensostuff/ONI_v4.shtml.
- Navarro-Gonzalez, R., 2003. Mars-like soils in the Atacama desert, Chile, and the dry limit of microbial life. *Science* 302, 1018–1021. <https://doi.org/10.1126/science.1089143>.
- Newberg, J.T., Matthew, B.M., Anastasio, C., 2005. Chloride and bromide depletions in sea-salt particles over the northeastern Pacific Ocean. *J. Geophys. Res. Atmos.* 110. <https://doi.org/10.1029/2004JD005446>. n/a-n/a.
- NOAA Climate Data Online Database, 2018. <https://www7.ncdc.noaa.gov/CDO>.
- Norman, A.L., Barrie, L.A., Toom-Sauntry, D., Sirois, A., Krouse, H.R., Li, S.M., Sharma, S., 1999. Sources of aerosol sulphate at Alert: apportionment using stable isotopes. *J. Geophys. Res. Atmos.* 104, 11619–11631. <https://doi.org/10.1029/1999JD900078>.
- O'dowd, C.D., De Leeuw, G., O'dowd, C.D., De Leeuw, G., 2007. Marine aerosol production: a review of the current knowledge. *Philos. Trans. R. Soc. London A Math. Phys. Eng. Sci.* 365. <https://doi.org/10.1098/rsta.2007.2043>.
- Osterloo, M.M., Hamilton, V.E., Bandfield, J.L., Glotch, T.D., Baldridge, A.M., Christensen, P.R., Tornabene, L.L., Anderson, F.S., 2008. Chloride-bearing materials in the southern highlands of Mars. *Science* 319, 1651–1654 (80-).
- Pachon, J.E., Weber, R.J., Zhang, X., Mulholland, J.A., Russell, A.G., 2013. Revising the use of potassium (K) in the source apportionment of PM_{2.5}. *Atmos. Pollut. Res.* 4, 14–21.
- Pan, Y.P., Wang, Y.S., 2015. Atmospheric wet and dry deposition of trace elements at 10 sites in Northern China. *Atmos. Chem. Phys.* 15 (2), 951–972.
- Patris, N., Cliff, S.S., Quinn, P.K., Kasem, M., Thiemens, M.H., 2007. Isotopic analysis of aerosol sulfate and nitrate during ITCT-2k2: determination of different formation pathways as a function of particle size. *J. Geophys. Res.* 112, D23301. <https://doi.org/10.1029/2005JD006214>.
- Pérez-Fodich, A., Reich, M., Álvarez, F., Snyder, G.T., Schoenberg, R., Vargas, G., Muramatsu, Y., Fehn, U., 2014. Climate change and tectonic uplift triggered the formation of the Atacama Desert's giant nitrate deposits. *Geology* 42, 251–254.
- Pilson, M.E.Q., 2012. *An Introduction to the Chemistry of the Sea*. Cambridge University Press.
- Rech, J.A., Quade, J., Hart, W.S., 2003. Isotopic evidence for the source of Ca and S in soil gypsum, anhydrite and calcite in the Atacama Desert, Chile. *Geochim. Cosmochim. Acta* 67, 575–586. [https://doi.org/10.1016/S0016-7037\(02\)01175-4](https://doi.org/10.1016/S0016-7037(02)01175-4).
- Rees, C.E., Jenkins, W.J., Monster, J., 1978. The sulphur isotopic composition of ocean water sulphate. *Geochim. Cosmochim. Acta* 42, 377–381.
- Reheis, M.C., 1997. Dust deposition downwind of Owens (dry) Lake, 1991–1994: preliminary findings. *J. Geophys. Res. Atmos.* 102, 25999–26008.
- Reheis, M.C., Kihl, R., 1995. Dust deposition in southern Nevada and California, 1984–1989: relations to climate, source area, and source lithology. *J. Geophys. Res. Atmos.* 100, 8893–8918. <https://doi.org/10.1029/94JD03245>.
- Risacher, F., Fritz, B., Hauser, A., 2011. Origin of components in Chilean thermal waters.

- J. S. Am. Earth Sci. 31, 153–170.
- Ropelewski, C.F., Halpert, M.S., 1989. Precipitation patterns associated with the high index phase of the Southern Oscillation. *J. Clim.* 2, 268–284.
- Rutllant, J.A., Muñoz, R.C., Garreaud, R.D., 2013. Meteorological observations on the northern Chilean coast during VOCALS-REx. *Atmos. Chem. Phys.* 13, 3409–3422.
- Sanusi, Astrid A., Norman, Ann-Lise, Burridge, Carolyn, Wadleigh, Moire, Tang, W.-W., 2006. Determination of the S Isotope Composition of Methanesulfonic Acid. <https://doi.org/10.1021/AC0600048>.
- Sargent, R., Bartley, C., Dille, P., Keller, J., Nourbakhsh, I., LeGrand, R., 2010. Timelapse GigaPan: capturing, sharing, and exploring timelapse gigapixel imagery. In: *Fine International Conference on Gigapixel Imaging for Science*.
- Schemenauer, R.S., Cereceda, P., Schemenauer, R.S., Cereceda, P., 1992. The quality of fog water collected for domestic and agricultural use in Chile. *J. Appl. Meteorol.* 31, 275–290.
- Schindler, D.W., Dillon, P.J., Schreier, H., 2006. A review of anthropogenic sources of nitrogen and their effects on Canadian aquatic ecosystems. In: *Nitrogen Cycling in the Americas: Natural and Anthropogenic Influences and Controls*. Springer, pp. 25–44.
- Seinfeld, J.H., Pandis, S.N., Noone, K., 1998. *Atmospheric Chemistry and Physics: From Air Pollution to Climate Change*.
- Sernageomin, 1982. *Mapa Geológico de Chile*.
- Shao, Y., Raupach, M.R., Findlater, P.A., 1993. Effect of saltation bombardment on the entrainment of dust by wind. *J. Geophys. Res.* 98, 12719. <https://doi.org/10.1029/93JD00396>.
- Sillitoe, R.H., Mortimer, C., Clark, A.H., 1968. A chronology of landform evolution and supergene mineral alteration, southern Atacama Desert, Chile. *Inst. Min. Metall. Trans. (Section B)* 27, 166–169.
- Singh, H.B., Hanst, P.L., 1981. Peroxyacetyl nitrate (PAN) in the unpolluted atmosphere: an important reservoir for nitrogen oxides. *Geophys. Res. Lett.* 8, 941–944.
- Singh, H.B., Salas, L.J., Ridley, B.A., Shetter, J.D., Donahue, N.M., Fehsenfeld, F.C., Fahey, D.W., Parrish, D.D., Williams, E.J., Liu, S.C., 1985. Relationship Between Peroxyacetyl Nitrate and Nitrogen Oxides in the Clean Troposphere.
- Stern, J.C., Sutter, B., Freissinet, C., Navarro-González, R., McKay, C.P., Archer, P.D., ... Fairen, A.G., 2015. Evidence for indigenous nitrogen in sedimentary and aeolian deposits from the Curiosity rover investigations at Gale crater, Mars. *Proc. Natl. Acad. Sci.* 112 (14), 4245–4250.
- Stoertz, G.E., Ericksen, G.E., 2009. *Geology of Salars in Northern Chile*.
- Ta, W., Xiao, H., Qu, J., Xiao, Z., Yang, G., Wang, T., Zhang, X., 2004. Measurements of dust deposition in Gansu Province, China, 1986–2000. *Geomorphology* 57, 41–51. [https://doi.org/10.1016/S0169-555X\(03\)00082-5](https://doi.org/10.1016/S0169-555X(03)00082-5).
- Tedeschi, G., Van Eijk, A.M.J., Piazzola, J., Kusmierczyk-Michulec, J.T., 2017. Influence of the surf zone on the marine aerosol concentration in a coastal area. *Boundary-layer Meteorol* 163, 327–350.
- U.S. Geological Survey, 2005. *Mineral resources data system: U.S. Geological Survey, Reston, Virginia*. https://mrdata.usgs.gov/mrds/show-mrds.php?dep_id=10079698.
- Valdés-Pineda, R., Valdés, J.B., Díaz, H.F., Pizarro-Tapia, R., 2016. Analysis of spatio-temporal changes in annual and seasonal precipitation variability in South America-Chile and related ocean-atmosphere circulation patterns. *Int. J. Climatol.* 36, 2979–3001.
- Van Driessche, A.E.S., Canals, A., Ossorio, M., Reyes, R.C., García-Ruiz, J.M., 2016. Unraveling the sulfate sources of (giant) gypsum crystals using gypsum isotope fractionation factors. *J. Geol.* 124, 235–245. <https://doi.org/10.1086/684832>.
- Vítek, P., Jehlička, J., Edwards, H.G.M., Hutchinson, I., Ascaso, C., Wierzchos, J., 2012. The miniaturized Raman system and detection of traces of life in halite from the Atacama desert: some considerations for the search for life signatures on mars. *Astrobiology* 12, 1095–1099. <https://doi.org/10.1089/ast.2012.0879>.
- Wadleigh, M.A., 2004. Sulphur isotopic composition of aerosols over the western North Atlantic Ocean. *Can. J. Fish. Aquat. Sci.* 61, 817–825. <https://doi.org/10.1139/f04-073>.
- Wang, F., Michalski, G., Seo, J. Hye, Ge, W., 2014. Geochemical, isotopic, and mineralogical constraints on atmospheric deposition in the hyper-arid Atacama Desert, Chile. *Geochim. Cosmochim. Acta* 135, 29–48. <https://doi.org/10.1016/j.gca.2014.03.017>.
- Wang, F., Michalski, G., Seo, J.-H., Granger, D.E., Lifton, N., Caffee, M., 2015. Beryllium-10 concentrations in the hyper-arid soils in the Atacama Desert, Chile: Implications for arid soil formation rates and El Niño driven changes in Pliocene precipitation. *Geochim. Cosmochim. Acta* 160, 227–242.
- Watts, D., Durán, P., Flores, Y., 2017. How does El Niño Southern Oscillation impact the wind resource in Chile? A techno-economical assessment of the influence of El Niño and La Niña on the wind power. *Renew. Energy* 103, 128–142. <https://doi.org/10.1016/j.renene.2016.10.031>.
- Wood, S., Cowie, A., 2004. A review of greenhouse gas emission factors for fertiliser production. In: *IEA Bioenergy Task*, pp. 1–20.
- Zakey, A.S., Giorgi, F., Bi, X., 2008. Modeling of sea salt in a regional climate model: Fluxes and radiative forcing. *J. Geophys. Res. Atmos.* 113.
- Zhang, B., Zhong, Z., Xue, Z., Xue, J., Xu, Y., 2018. Release and transformation of potassium in co-combustion of coal and wheat straw in a BFB reactor. *Appl. Therm. Eng.* 144, 1010–1016.